Optimal Disturbances in Compressible Boundary Layers – Complete Energy Norm Analysis

Simone Zuccher* and Anatoli Tumin†
University of Arizona, Tucson, AZ, 85721, USA
Eli Reshotko‡
Case Western Reserve University, Cleveland, OH, 44106, USA

In the present work we revise results of transient growth in compressible boundary layers (flat plate and sphere) to consider the complete Mack energy norm at the outlet, without the assumption that the outflow perturbation is comprised solely of streaky structures. Optimal perturbations are still in the form of counter-rotating streamwise vortices and this justifies the choice of the scaling in the governing equations. A strong effect of the complete (full) energy norm at the outlet is found for the flat plate in supersonic regimes. No significant effects of the choice of the outlet norm can be appreciated for the sphere, in the range of parameters that are relevant to wind tunnel testing or flight conditions.

Nomenclature

$\boldsymbol{A}, \boldsymbol{B}, \boldsymbol{C}$		y	distance from the wall
$\boldsymbol{D}, \boldsymbol{H}, \boldsymbol{M}, \widetilde{\boldsymbol{M}}$	matrices	z	spanwise coordinate
E	energy of the perturbation	β	spanwise wavenumber
$\mathbf{f}$	vector of unknowns	γ	specific heat ratio
G	energy ratio parameter	ν	kinematic viscosity
i	$\sqrt{-1}$	θ	meridional angle
$\mathcal{L}$	augmented functional	ρ	density
M	Mach number		
p	pressure	*Subscripts*	
$\mathbf{p}$	vector of adjoint variables	ad	adiabatic conditions
Pr	Prandtl number	e	edge of the boundary layer
R	sphere radius	in	inlet conditions
Re	Reynolds number	out	outlet conditions
T	temperature	s	basic state
u	streamwise velocity component	w	wall conditions
v	wall-normal velocity component		
w	spanwise velocity component	*Subscripts*	
x	streamwise coordinate	ad	adiabatic conditions

I. Introduction

The problem of optimal disturbances, in the context of bypass transition to turbulence, has been of great interest during the last decade. There are many applications where transition to turbulence occurs without

*Research Assistant Professor, Department of Aerospace and Mechanical Engineering, AIAA Member.
†Associate Professor, Department of Aerospace and Mechanical Engineering, AIAA Senior Member.
‡Kent H. Smith Professor Emeritus of Engineering, Department of Mechanical and Aerospace Engineering, AIAA Fellow.

exponential growth, but where there is great potential for transient growth of the disturbance energy in flows that are stable to wave-like perturbations (Tollmien–Schlichting waves).

Transient growth arises from the coupling between slightly damped, highly oblique Orr-Sommerfeld and Squire modes leading to algebraic growth followed by exponential decay in subcritical regions outside the Tollmien-Schlichting neutral curve. A weak transient growth can also occur for two-dimensional modes since the Orr-Sommerfeld operator and its compressible counterpart are not self-adjoint, and therefore their eigenfunctions are not strictly orthogonal.[1]

Historically, the first approach to nonmodal disturbances was in the inviscid limit. It was found that the streamwise disturbance velocity amplitude may grow algebraically in time, even though the basic flow does not posses an inflection point.[2] It was also showed that all parallel inviscid shear flows are unstable to a wide class of three-dimensional disturbances[3] and the result is independent of whether or not the shear flow is unstable to exponential growth. The temporal analysis of the evolution of a three-dimensional disturbance in a boundary layer[4] revealed an initial algebraic growth followed by a viscous decay (transient growth). In Ref. 5 optimal perturbations were first so named to denote the initial flow disturbances that produced the maximum gain, defined as the ratio between the perturbation kinetic energies at the final and initial time. A similar concept had, however, already been introduced for flow in a pipe.[6] The first quantitative calculation of three–dimensional optimal perturbations with respect to temporal growth for a parallel approximation of the Blasius boundary layer can be found in Ref. 7. Other works,[8,9,10] carried out more than a decade ago, recognized the great potential of nonmodal growth for explaining bypass transition.

Optimal perturbations in the spatial framework have only more recently been considered. The spatial Cauchy problem within the scope of the linearized Navier–Stokes equations is, however, radically different from the temporal one and ill posed. This is the main obstacle in applying to the spatial analysis the same optimization methods used in the temporal case. The problem rises from the presence of modes with a negative imaginary part of the streamwise wavenumber α. These are modes decaying upstream and associated with the downstream boundary conditions. In Ref. 11 it was pointed out that if the downstream boundary is moved far away, the upstream decaying modes can be neglected and the optimization can be carried out within the scope of the Cauchy problem, similarly to the temporal analysis. The ill-posedness of the spatial Cauchy problem was first overcome by considering the (linearized) boundary layer equations[12,13] instead of the Navier–Stokes equations. In addition, nonparallel effects were included. It was found that the optimal initial disturbance is composed of stationary streamwise vortices whereas the induced velocity field is dominated by streamwise streaks. The maximum amplification occurs in the steady case (frequency $\omega = 0$) and for a non-zero value of the spanwise wavenumber $\beta = 0.45$ (scaled with $l = \sqrt{\nu L/U_\infty}$, ν being the kinematic viscosity, U_∞ the freestream velocity and L the longitudinal distance from the leading edge to the location where output energy is maximized). In the spatial framework, optimal perturbations have also been computed in the nonlinear case.[14]

The compressible counterpart of the aforementioned works has also been considered. Temporal[15] and spatial[16,11,17] analyses of the transient growth phenomenon have been carried out within the scope of parallel flow approximation. A model for transient growth including non-parallel effects in the compressible boundary layer past a flat plate has also been developed.[18]

Compressible optimal perturbations calculated by including surface curvature effects and non-parallel growth of the boundary layer are still missing and can actually be of great importance to explain the long-standing blunt body paradox.[16] Depending on the choice of the norm, which states what quantity will be maximized, constrained optimization in the framework of optimal perturbation can lead to quite different results. In the incompressible framework, full inlet energy norm[12] and energy norm including only the spanwise and wall-normal velocity components[13] were employed. In Ref. 12 both norms at the inlet and at the outlet depend on the Reynolds number Re. However, in the limit $Re \to \infty$ (practically for $Re > 10^4$) results collapse on those obtained in Ref. 13.

The choice of the energy norm, therefore, can be a delicate issue, especially in the compressible case where effects due to compressibility should be taken into account through the inclusion of density and temperature. The physics of transient growth is mainly dominated by streamwise vortices[12,13] and therefore the choice of an initial energy excluding the streamwise velocity component, in the fashion proposed in Ref. 13, is satisfactory. The choice of an outlet norm including only temperature and the component of the velocity in the streamwise direction, however, might not represent completely the structure of the flow field if the flow is not dominated by streamwise streaks. This could be the case of a blunt body, for which there are some indications that the largest transient growth is located close to the stagnation point.[19] Due to the

short interval in the streamwise direction, a flow field mainly dominated by streaks might not be completely established and thus the contribution of the wall-normal and spanwise velocity components to the energy norm at the outlet could be non negligible.

The objective of the present work is therefore twofold. In the framework of compressible optimal perturbations, the use of a full energy norm at the outlet is considered and compared with the use of a partial energy norm. Curvature effects are included in order to investigate optimal disturbances developing in the compressible, non-parallel boundary layer over a sphere.

II. Governing equations

Governing equations for the steady, three-dimensional disturbance in a compressible flow are derived from the linearized Navier–Stokes equations.

A small parameter $\epsilon = H_{\rm ref}/L_{\rm ref}$ is introduced for scaling purposes, where $H_{\rm ref} = \sqrt{\nu_{\rm ref} L_{\rm ref}/U_{\rm ref}}$ is a typical boundary layer length in the wall-normal direction y and $L_{\rm ref}$ is a typical scale of the geometry (length of the flat plate L, radius of the sphere R, etc.). In the case of the flat plate $H_{\rm ref} = l = \sqrt{\nu_\infty L/U_\infty}$ (the subscript ∞ stands for freestream parameters, outside the boundary layer), while for the sphere $H_{\rm ref} = \sqrt{\nu_{\rm ref} R/U_{\rm ref}}$ where the reference quantities are the values at the edge of the boundary layer at a certain downstream location $x_{\rm ref}$, x being the streamwise direction. The scaling parameter ϵ is thus strictly related to the Reynolds number Re. For the flat plate $\epsilon = Re_L^{-1/2}$, where $Re_L = U_\infty L/\nu_\infty$ is the Reynolds number based on the length of the plate and freestream conditions, while for the sphere $\epsilon = Re_{\rm ref}^{-1/2}$, where $Re_{\rm ref} = U_{\rm ref} R/\nu_{\rm ref}$ is the reference Reynolds number based on the radius of the sphere R and reference parameters.

As it follows from previous works regarding optimal perturbations in both incompressible and compressible boundary layers,[13,20,17,14,21] the disturbance flow is expected to be dominated by streamwise vortices and therefore the following scaling is employed. The streamwise coordinate x is normalized with $L_{\rm ref}$, whereas the wall-normal coordinate y and the spanwise coordinate z are scaled with $\epsilon L_{\rm ref}$. The streamwise velocity component u is scaled with $U_{\rm ref}$, wall-normal velocity v and spanwise velocity w with $\epsilon U_{\rm ref}$, temperature T with $T_{\rm ref}$ and pressure p with $\epsilon^2 \rho_{\rm ref} U_{\rm ref}^2$. Density ρ is eliminated through the state equation.

Due to the scaling adopted, the second derivative with respect to the streamwise coordinate x is smaller than the other terms, and is therefore neglected. This leads to a change in the nature of the equations from elliptic (Navier–Stokes equations) to parabolic.

For the flat plate, perturbations are assumed to be periodic in z, so that a general variable can be expressed as $q(x,y)\exp(\mathrm{i}\beta z)$, where $q(x,y)$ is the amplitude, which depends on x and y, β is the spanwise wavenumber and i is the imaginary unit. Similarly, for the sphere, perturbations are assumed to be periodic in the azimuthal direction ϕ as $\exp(\mathrm{i}m\phi)$, where m is the azimuthal index.

If the vector of perturbations is $\mathbf{f} = [u, v, w, T, p]^{\rm T}$ (where the superscript $^{\rm T}$ denotes the transpose), with $w = \mathrm{i}\tilde{w}$ ($\tilde{w}$ being the amplitude of the spanwise velocity component), the governing equations can be written as follows:[18]

$$(\boldsymbol{A}\mathbf{f})_x = (\boldsymbol{D}\mathbf{f}_y)_x + \boldsymbol{B}_0\mathbf{f} + \boldsymbol{B}_1\mathbf{f}_y + \boldsymbol{B}_2\mathbf{f}_{yy} \tag{1}$$

This form of the governing equations is general and can be derived for different geometries such as flat plate, sphere, sharp cone or blunt-nose cone. Nonzero elements of the 5 by 5 real matrices $\boldsymbol{A}$, $\boldsymbol{B}_0$, $\boldsymbol{B}_1$, $\boldsymbol{B}_2$ and $\boldsymbol{D}$ for the flat plate are defined in the appendix of Ref. 18, while for the sphere they are reported in the appendix of Ref. 17.

As far as boundary conditions are concerned, all perturbations are required to be zero at the wall except for p, while in the freestream all perturbations vanish except for v:

$$\begin{aligned} y = 0: &\quad u = 0; v = 0; w = 0; T = 0 \\ y \to \infty: &\quad u \to 0; w \to 0; p \to 0; T \to 0 \end{aligned} \tag{2}$$

In order to isolate the derivative with respect to x, system (1) can be recast in a simple form as

$$(\boldsymbol{H}_1\mathbf{f})_x + \boldsymbol{H}_2\mathbf{f} = 0 \tag{3}$$

where operators $\boldsymbol{H}_1$ and $\boldsymbol{H}_2$ are still 5 by 5 real matrices and contain the dependence on x and y due to the basic flow:

$$\boldsymbol{H}_1 = \boldsymbol{A} - \boldsymbol{D}(\cdot)_y; \qquad \boldsymbol{H}_2 = -\boldsymbol{B}_0 - \boldsymbol{B}_1(\cdot)_y - \boldsymbol{B}_2(\cdot)_{yy} \tag{4}$$

System (3) is parabolic in nature and can be solved by means of a downstream marching procedure with initial data specified at the inlet section of the domain $x = x_{\text{in}}$.

It is worth noting that, due to the normalization chosen, the disturbance equations for the flat plate are Reynolds number independent, i.e. Reynolds number Re does not enter explicitly in the equations, while for the sphere they are not Reynolds number independent due to the parameter ϵ in the scaling, which is associated with curvature effects.

III. Constrained optimization and adjoint discrete equations

As stated in the introduction, we are interested in finding initial optimal disturbances for the compressible boundary layer over a flat plate and a sphere. The term "optimal" here refers to the initial condition that is able to produce the worst possible scenario as far as transition is concerned. It is clear that the choice of a specific quantity that can measure this worst possible scenario is neither easy nor unique. In previous works dealing with optimal perturbations in the incompressible framework,[12,13,20,14,21] the kinetic energy of the disturbance field has always been the choice.

Once the objective function has been identified, the Lagrangian multiplier technique is employed in order to solve the constrained optimization problem. In doing so the costate or adjoint equations are derived. If this is applied to the discrete equations, the discrete version of the adjoint problem is obtained. The procedure is outlined for a general case, as done in §II.

A. The objective function

In problems related to boundary-layer transition, the quantity that monitors the instability development is typically the kinetic energy. In optimal perturbation studies the latter is usually maximized at the outlet of the computational domain, but in other cases the integral of the kinetic energy over the whole domain has been considered, especially for optimal control problems.[20,14] Since one of the goals of the present study is to check how the use of a "full energy norm" at the outlet can influence the results, the expression we choose to maximize is Mack's energy norm[22] of the perturbation kinetic energy and temperature in the outlet plane,

$$E_{\text{out}} = \int_0^\infty \left[\rho_{s\text{out}} (u_{\text{out}}^2 + v_{\text{out}}^2 + w_{\text{out}}^2) + \frac{\rho_{\text{out}}^2 T_{s\text{out}}}{\gamma \rho_{s\text{out}} M^2} + \frac{T_{\text{out}}^2 \rho_{s\text{out}}}{\gamma(\gamma-1) T_{s\text{out}} M^2} \right] dy. \tag{5}$$

Expression (5) was derived for perturbations in the boundary layer over a flat plate within the temporal framework and is here utilized for the spatial one, as done in Ref. 18 (for the sphere, the integration generates a slightly different expression for the energy norm, which can be found in Appendix of Ref. 17). After employing the equation of state for the basic flow and for the perturbation and normalizing p according to the scaling in §II, the norm reads

$$E_{\text{out}} = \int_0^\infty \left[\rho_{s\text{out}} (u_{\text{out}}^2 + v_{\text{out}}^2 + w_{\text{out}}^2) + \frac{p_{s\text{out}} T_{\text{out}}^2}{(\gamma-1) T_{s\text{out}}^2 M^2} \right] dy \tag{6}$$

and can be more compactly recast in matrix form as

$$E_{\text{out}} = \int_0^\infty \left(\mathbf{f}_{\text{out}}^T \widetilde{\boldsymbol{M}}_{\text{out}} \mathbf{f}_{\text{out}} \right) dy \tag{7}$$

where the linear operator $\widetilde{\boldsymbol{M}}_{\text{out}}$ is a diagonal 5×5 matrix

$$\widetilde{\boldsymbol{M}}_{\text{out}} = \begin{bmatrix} \rho_{s\text{out}} & 0 & 0 & 0 & 0 \\ 0 & \rho_{s\text{out}} & 0 & 0 & 0 \\ 0 & 0 & \rho_{s\text{out}} & 0 & 0 \\ 0 & 0 & 0 & \dfrac{p_{s\text{out}}}{(\gamma-1) T_{s\text{out}}^2 M^2} & 0 \\ 0 & 0 & 0 & 0 & 0 \end{bmatrix}. \tag{8}$$

The initial condition is arbitrary, in the sense that in principle we can assign all five variables at x_{in}. However, in Ref. 13 it was observed that for the incompressible case, in the $Re \to \infty$ limit, the choice $u_{\text{in}} = 0$, $p_{\text{in}} = 0$, v_{in} and w_{in} related by the continuity equations guarantees the maximum gain in an input-output fashion. This choice also correspond to the physical mechanism, observed in transitional boundary layer flows, known as the lift-up effect,[3] according to which streamwise vortices lift low momentum flow up (from the wall) and push down high momentum flow causing streaks that eventually break down to turbulence. Led by these considerations, here we focus on initial perturbations with only v and w nonzero, which correspond to steady, streamwise vortices. It should be noticed, however, that in the case of finite Reynolds number, for example $Re = 1000$, and for the incompressible boundary layer past a flat plate, the choice of a full energy norm at both inlet and outlet guarantees the largest gain in the optimization.[12]

The kinetic energy of the optimal disturbance $\mathbf{f}_{\text{in}}$, if only v_{in} and w_{in} are nonzero, is therefore:

$$E_{\text{in}} = \int_0^\infty \left[\rho_{s_{\text{in}}}(v_{\text{in}}^2 + w_{\text{in}}^2)\right] dy, \tag{9}$$

or more compactly

$$E_{\text{in}} = \int_0^\infty \left(\mathbf{f}_{\text{in}}^T \widetilde{\boldsymbol{M}}_{\text{in}} \mathbf{f}_{\text{in}}\right) dy \tag{10}$$

where $\widetilde{\boldsymbol{M}}_{\text{in}}$ is a 5×5 diagonal matrix

$$\widetilde{\boldsymbol{M}}_{\text{in}} = \begin{bmatrix} 0 & 0 & 0 & 0 & 0 \\ 0 & \rho_{s_{\text{in}}} & 0 & 0 & 0 \\ 0 & 0 & \rho_{s_{\text{in}}} & 0 & 0 \\ 0 & 0 & 0 & 0 & 0 \\ 0 & 0 & 0 & 0 & 0 \end{bmatrix} \tag{11}$$

Since the problem is linear, we can choose a certain normalization for the initial disturbance at x_{in}, e.g. $E_{\text{in}} = E_0 = 1$.

From the above discussion it is clear that the whole problem of finding optimal perturbations reduces to a "constrained optimization", in which we seek the initial conditions for the disturbance equations (3) that maximize (7) and that satisfy the constraint $E_{\text{in}} = E_0$ at x_{in} together with the direct equations (3) and boundary conditions (2) at each $x \in (x_{\text{in}}; x_{\text{out}})$.

B. Constrained optimization

The classical Lagrange multiplier technique is one of the most known tools to solve constrained optimization problems. As applied to optimal perturbations, numerous examples can be found in the literature regarding the continuous version of such an approach, which leads to the so-called adjoint equations in a continuous fashion. Rigorously speaking, in the theory of linear operators the adjoint equations are derived by satisfying an equality involving an inner product.[23,24] Therefore their form is not necessarily related to constrained optimization problems. On the contrary, when the adjoint equations are derived from a constrained optimization (as in our case) only if the objective function includes exclusively quantities at the boundaries of the domain then their form is the same as those derived from an inner product equality. In fact, if we try to maximize the integral of the energy over the whole domain (as opposed to the outlet energy only), a source term arises in the adjoint equations.[20,14,21] Less numerous are the examples where the Lagrange multiplier technique is applied directly to the discrete equations.[25,26,13,20,14,21]

The use of the discrete approach has several advantages among which the necessity of an "ad hoc" adjoint code is avoided and a foolproof test is available by comparing the results of the direct and adjoint calculation, which must match up to machine accuracy for any step size and not only in the limit of step size tending to zero.[21] This is due to the conservation of a quantity which depends on x only.[25,13] For a thorough discussion on the issue of continuous versus discrete adjoints the reader is referred to Ref. 27.

The numerical discretization of a general parabolic system of partial differential equations such as (3) can always be recast as

$$\boldsymbol{C}_{n+1}\mathbf{f}_{n+1} = \boldsymbol{B}_n\mathbf{f}_n \tag{12}$$

where n denotes the n-th grid point in the streamwise direction x, $\mathbf{f}$ is the vector of unknowns (not with only 5 elements but with $5 \times N_y$, where N_y is the number of grid points in the wall-normal direction y) and matrices $\boldsymbol{C}$ and $\boldsymbol{B}$ depend on x (as the basic flow does) and account for the discretization in both x and y. The solution is found by marching forward in space from $n = 0$ (x_{in}), given the initial condition $\mathbf{f}_0$, to $n = N$ (x_{out}). The boundary conditions at the wall and for $y \to \infty$ are already included in the matrices rows. The discrete objective function we aim to maximize is $\mathcal{J} = \mathbf{f}_N^{\mathrm{T}}\boldsymbol{M}_N\mathbf{f}_N$, where $\boldsymbol{M}_N$ is the discrete version of $\widetilde{\boldsymbol{M}}_{\text{out}}$ as defined in (7) and accounts for the discretization of the integral in y.

The augmented functional $\mathcal{L}$, which contains the objective function $\mathcal{J} = E_{\text{out}}$, the constraints (12) and $E_{\text{in}} = E_0$, and the Lagrange multipliers, is written as

$$\mathcal{L}(\mathbf{f}_0, \ldots, \mathbf{f}_N) = \mathbf{f}_N^{\mathrm{T}}\boldsymbol{M}_N\mathbf{f}_N + \sum_{n=0}^{N-1}\left[\mathbf{p}_n^{\mathrm{T}}\left(\boldsymbol{C}_{n+1}\mathbf{f}_{n+1} - \boldsymbol{B}_n\mathbf{f}_n\right)\right] + \lambda_0[\mathbf{f}_0^{\mathrm{T}}\boldsymbol{M}_0\mathbf{f}_0 - E_0] \tag{13}$$

where $\mathbf{p}_n$ is the vector of Lagrangian multipliers, which depends on the streamwise location n and $\boldsymbol{M}_0$ is the discrete version of $\widetilde{\boldsymbol{M}}_{\text{in}}$ as defined in (10), in the same fashion as $\boldsymbol{M}_N$. Only the dependence on $\mathbf{f}_n$ ($n = 0, \ldots, N$) has been emphasized in $\mathcal{L}$ because its derivative with respect to the Lagrangian multipliers (which is needed to impose $\delta\mathcal{L} = 0$) would lead to the constraints, that are already known. The summation between 0 and $N-1$ in (13) involving $\mathbf{p}_n$ reflects the integral along x. The integration by parts (which would be performed in the continuous case) is here replaced by adding and subtracting $\mathbf{p}_{n+1}^{\mathrm{T}}\boldsymbol{B}_{n+1}\mathbf{f}_{n+1}$ in the summation so that the terms can be rearranged as

$$\begin{aligned}
\sum_{n=0}^{N-1}\left[\mathbf{p}_n^{\mathrm{T}}\left(\boldsymbol{C}_{n+1}\mathbf{f}_{n+1} - \boldsymbol{B}_n\mathbf{f}_n\right)\right] &= \sum_{n=0}^{N-1}\left[\mathbf{p}_n^{\mathrm{T}}\boldsymbol{C}_{n+1}\mathbf{f}_{n+1} - \mathbf{p}_{n+1}^{\mathrm{T}}\boldsymbol{B}_{n+1}\mathbf{f}_{n+1}\right] + \\
&\quad \sum_{n=0}^{N-1}\left[\mathbf{p}_{n+1}^{\mathrm{T}}\boldsymbol{B}_{n+1}\mathbf{f}_{n+1} - \mathbf{p}_n^{\mathrm{T}}\boldsymbol{B}_n\mathbf{f}_n\right] \\
&= \sum_{n=0}^{N-1}\left[\mathbf{p}_n^{\mathrm{T}}\boldsymbol{C}_{n+1}\mathbf{f}_{n+1} - \mathbf{p}_{n+1}^{\mathrm{T}}\boldsymbol{B}_{n+1}\mathbf{f}_{n+1}\right] + \\
&\quad \mathbf{p}_N^{\mathrm{T}}\boldsymbol{B}_N\mathbf{f}_N - \mathbf{p}_0^{\mathrm{T}}\boldsymbol{B}_0\mathbf{f}_0,
\end{aligned}$$

and expression (13) can be rewritten as

$$\begin{aligned}
\mathcal{L}(\mathbf{f}_0, \ldots, \mathbf{f}_N) &= \mathbf{f}_N^{\mathrm{T}}\boldsymbol{M}_N\mathbf{f}_N + \sum_{n=0}^{N-1}\left[\mathbf{p}_n^{\mathrm{T}}\boldsymbol{C}_{n+1}\mathbf{f}_{n+1} - \mathbf{p}_{n+1}^{\mathrm{T}}\boldsymbol{B}_{n+1}\mathbf{f}_{n+1}\right] + \\
&\quad \mathbf{p}_N^{\mathrm{T}}\boldsymbol{B}_N\mathbf{f}_N - \mathbf{p}_0^{\mathrm{T}}\boldsymbol{B}_0\mathbf{f}_0 + \lambda_0[\mathbf{f}_0^{\mathrm{T}}\boldsymbol{M}_0\mathbf{f}_0 - E_0].
\end{aligned} \tag{14}$$

As in the continuous case, the stationary condition is found when $\delta\mathcal{L} = 0$

$$\frac{\delta\mathcal{L}}{\delta\mathbf{f}_0}\delta\mathbf{f}_0 + \sum_{n=0}^{N-2}\left[\frac{\delta\mathcal{L}}{\delta\mathbf{f}_{n+1}}\delta\mathbf{f}_{n+1}\right] + \frac{\delta\mathcal{L}}{\delta\mathbf{f}_N}\delta\mathbf{f}_N = 0,$$

which, in order to be satisfied for any arbitrary $\mathbf{f}_0$, $\mathbf{f}_{n+1}$ and $\mathbf{f}_N$, leads to

$$\frac{\delta\mathcal{L}}{\delta\mathbf{f}_0} = -\mathbf{p}_0^{\mathrm{T}}\boldsymbol{B}_0 + 2\lambda_0\mathbf{f}_0^{\mathrm{T}}\boldsymbol{M}_0 = 0 \tag{15}$$

$$\frac{\delta\mathcal{L}}{\delta\mathbf{f}_{n+1}} = \mathbf{p}_n^{\mathrm{T}}\boldsymbol{C}_{n+1} - \mathbf{p}_{n+1}^{\mathrm{T}}\boldsymbol{B}_{n+1} = 0, \quad n = 0, \ldots, N-2 \tag{16}$$

$$\frac{\delta\mathcal{L}}{\delta\mathbf{f}_N} = 2\mathbf{f}_N^{\mathrm{T}}\boldsymbol{M}_N + \mathbf{p}_N^{\mathrm{T}}\boldsymbol{B}_N = 0 \tag{17}$$

Equation (15) furnishes the optimality condition to be satisfied at x_{in} and equation (16) leads to

$$\mathbf{p}_n^{\mathrm{T}}\boldsymbol{C}_{n+1} - \mathbf{p}_{n+1}^{\mathrm{T}}\boldsymbol{B}_{n+1} = 0, \tag{18}$$

which is the discrete form of the adjoint equations to be solved by marching backwards from x_{out} to x_{in} with the initial condition provided by equation (17) solved for $\mathbf{p}_N$.

1. *Outlet conditions*

From expression (17) follows

$$\boldsymbol{B}_N^{\mathrm{T}}\mathbf{p}_N = -2\boldsymbol{M}_N^{\mathrm{T}}\mathbf{f}_N \tag{19}$$

where $\boldsymbol{B}_N$ is the discrete representation of $\boldsymbol{H}_{1_{\mathrm{out}}}$ and is singular due to the fact that the fifth column in $\boldsymbol{H}_1$ is made of zeros as $p_x = 0$ in this approximation (the last column of matrix $\boldsymbol{A}$ is made of zeros). This implies that the solution cannot be found unless the solvability condition is satisfied. The singularity of $\boldsymbol{H}_1$ is not simply a practical numerical problem for the solution of (19) but contains deeper information and insights regarding the initial condition for the adjoint variables. The impossibility to determine a unique solution of (19) translates into the fact that at least one out of five adjoint variables is free at $x = x_{\mathrm{out}}$ and therefore can be chosen arbitrarily. For sake of simplicity, we set p_5 (the fifth adjoint variable) to zero.

2. *Inlet conditions*

By imposing $\delta\mathcal{L}/\delta\mathbf{f}_{\mathrm{in}} = 0$ condition (15) was obtained. The operator $\boldsymbol{M}_0$ is the discrete counterpart of $\boldsymbol{M}_{\mathrm{in}}$ and is singular (as $\boldsymbol{M}_{\mathrm{out}}$) so $\boldsymbol{M}_0^{-1}$ does not exist and (15) can not be solved. However, $\boldsymbol{M}_0$ is diagonal and therefore the j-th element of $\mathbf{f}_0$ corresponding to $\boldsymbol{M}_{0jj} \neq 0$ can be retrieved by

$$\mathbf{f}_{0_j} = \begin{cases} \dfrac{(\mathbf{p}_0^T\boldsymbol{B}_0)_j}{2\lambda\boldsymbol{M}_{0jj}} & \text{if} \quad \boldsymbol{M}_{0jj} \neq 0 \\ \\ 0 & \text{if} \quad \boldsymbol{M}_{0jj} = 0 \end{cases} \tag{20}$$

The multiplier λ is found by imposing $E_0 = E_{\mathrm{in}}$.

C. An optimization algorithm

The constrained optimization developed above has enabled us to write a set of equations and boundary conditions that must be satisfied simultaneously. More specifically, we first need to solve system (12) from $x = x_{\mathrm{in}}$ $(n = 0)$ to $x = x_{\mathrm{out}}$ $(n = N)$ with initial conditions at x_{in} expressed by (20). We refer to this as the direct or forward problem. Then we need to solve system (18) from $x = x_{\mathrm{out}}$ $(n = N)$ to $x = x_{\mathrm{in}}$ $(n = 0)$, with initial conditions derived from (19) and provided at $x = x_{\mathrm{out}}$. We call this the adjoint or backward problem.

A quite large system of linear equations supplemented by initial and boundary conditions has to be solved. Instead of doing it in one shot, however, we employ the intrinsic parabolic nature of the equations to efficiently solve separately the two coupled problems. Such an algorithm can be outlined in the following few steps:

1. a guessed initial condition $\mathbf{f}_{\mathrm{in}}^{(0)}$ is provided at the beginning of the optimization procedure
2. the forward problem (12) is solved at the n-th iteration with the initial condition $\mathbf{f}_{\mathrm{in}}^{(n)}$
3. the objective function $\mathcal{J}^{(n)} = E_{\mathrm{out}}^{(n)}$ is computed at the end of the forward iteration and compared to the objective function $\mathcal{J}^{(n-1)} = E_{\mathrm{out}}^{(n-1)}$ at the end of the previous forward iteration. If $|\mathcal{J}^{(n)}/\mathcal{J}^{(n-1)} - 1| < \epsilon_t$ (where ϵ_t is the maximum tolerance accepted to stop the optimization) then the optimization is considered converged
4. if $|\mathcal{J}^{(n)}/\mathcal{J}^{(n-1)} - 1| > \epsilon_t$ the initial conditions for the backward problem (19) are assigned at the outlet and derived from the direct solution at $x = x_{\mathrm{out}}$
5. the backward problem (18) is solved from $x = x_{\mathrm{out}}$ to $x = x_{\mathrm{in}}$
6. a new initial condition for the forward problem $\mathbf{f}_{\mathrm{in}}^{(n+1)}$ is obtained from the solution of the backward problem at $x = x_{\mathrm{in}}$ employing (20)
7. the loop is repeated from step 2 on

It should be noticed that the above procedure does not necessarily guarantee convergence. If there is an attractor for the solution, then the procedure will capture it and this happens quite fast (2-3 forward-backward iterations) when the norm proposed in Ref. 13 is used. On the other hand, it was observed that when the full energy norm is employed the convergence is generally much slower, depending on the wavenumber β, reaching the fastest convergence in the proximity of the optimal β.

IV. Discretization

A finite difference discretization scheme has been implemented to numerically solve the equations (3) with boundary conditions (2). For sake of generality, grid points in x and y are not necessarily equally spaced. A staggered grid is introduced in the wall-normal direction, with variables u, v, w and T known at the grid points, and p known at the mid-grid (staggered) points. All equations are satisfied at the grid points except for continuity, which is satisfied in the mid-grid points. The use of the uneven grid in y allows us to cluster more nodes close to the wall so as to take into account the large gradients of boundary layer quantities in this region.

The last point of the y-grid is located far enough from the wall to allow us to specify there the boundary conditions for $y \to \infty$.

Fourth-order non-compact finite differences are used for the y discretization, employing six points so as to allow 4th order accuracy for the second derivative. By using six points, the first derivative is automatically 5th order accurate and the function (when interpolated due to the staggered grid) is 6th order accurate.

Also the discretization in the streamwise direction is based on uneven grid. Since the system of boundary layer equations is parabolic, a second order backward discretization is chosen, which requires the solution at two previous steps to be known. For the first step, however, a first order scheme is used because only the initial condition is available.

After the discretization, the original system of partial differential equations (3) can be re-written in the following form:

$$\left[C^0_{n+1}\boldsymbol{H}^1_{n+1} + \boldsymbol{H}^2_{n+1}\right]\mathbf{f}_{n+1} = -C^1_{n+1}\boldsymbol{H}^1_n\mathbf{f}_n - C^2_{n+1}\boldsymbol{H}^1_{n-1}\mathbf{f}_{n-1} \tag{21}$$

where coefficients C^0_{n+1}, C^1_{n+1} and C^2_{n+1} account for the streamwise discretization and matrices $\boldsymbol{H}^1_{n+1}$ and $\boldsymbol{H}^2_{n+1}$ are the discretized version of respectively $\boldsymbol{H}_1$ and $\boldsymbol{H}_2$ introduced in §II. The solution is thus completely determined once the initial condition $\mathbf{f}_0 = \mathbf{f}_{\text{in}}$ is given at x_{in}. Clearly, for the first step in x a first-order approximation is used for the derivative since data are available only at one point upstream, not two.

Equation (21) can be easily rewritten in a form similar to (12)

$$\boldsymbol{C}_{n+1}\mathbf{f}_{n+1} = C^1_{n+1}\boldsymbol{B}_n\mathbf{f}_n + C^2_{n+1}\boldsymbol{B}_{n-1}\mathbf{f}_{n-1} \tag{22}$$

where $\boldsymbol{C}_{n+1} = \left[C^0_{n+1}\boldsymbol{H}^1_{n+1} + \boldsymbol{H}^2_{n+1}\right]$ and $\boldsymbol{B}_n = -\boldsymbol{H}^1_n$

Contrary to the simple form (12), which refers to a scheme where the new solution $\mathbf{f}_{n+1}$ depends on $\mathbf{f}_n$ only, the discrete equation (21) depends on $\mathbf{f}_n$ and $\mathbf{f}_{n-1}$ due to the second order approximation in x. Therefore, the discrete adjoint system is slightly different from (18). More specifically, by repeating the same steps as in §B, the constraint $\boldsymbol{C}_{n+1}\mathbf{f}_{n+1} - C^1_{n+1}\boldsymbol{B}_n\mathbf{f}_n - C^2_{n+1}\boldsymbol{B}_{n-1}\mathbf{f}_{n-1} = 0$ is left multiplied by the vector of Lagrangian multipliers $\mathbf{p}_n$ and then all terms are included in the summation on n (in the streamwise direction) to form the functional for the constrained optimization. Within this summation, we first add and subtract the quantity $\mathbf{p}^{\mathrm{T}}_{n+1}\left[C^1_{n+2}\boldsymbol{B}_{n+1}\mathbf{f}_{n+1} + C^2_{n+2}\boldsymbol{B}_n\mathbf{f}_n\right]$ and rearrange the summation as $\sum \mathbf{p}^{\mathrm{T}}_n\left[\boldsymbol{C}_{n+1}\mathbf{f}_{n+1}\right] - \sum \mathbf{p}^{\mathrm{T}}_{n+1}\left[C^1_{n+2}\boldsymbol{B}_{n+1}\mathbf{f}_{n+1} + C^2_{n+2}\boldsymbol{B}_n\mathbf{f}_n\right]$ and then we add and subtract the quantity $\mathbf{p}^{\mathrm{T}}_{n+2}\left[C^1_{n+3}\boldsymbol{B}_{n+1}\mathbf{f}_{n+1}\right]$ so that the final form of the summation is $\sum \mathbf{p}^{\mathrm{T}}_n\left[\boldsymbol{C}_{n+1}\mathbf{f}_{n+1}\right] - \sum \mathbf{p}^{\mathrm{T}}_{n+1}\left[C^1_{n+2}\boldsymbol{B}_{n+1}\mathbf{f}_{n+1}\right] - \sum \mathbf{p}^{\mathrm{T}}_{n+2}\left[C^2_{n+3}\boldsymbol{B}_{n+1}\mathbf{f}_{n+1}\right]$. In this way, all terms are right multiplied by $\mathbf{f}_{n+1}$ so that the derivative of the functional $\mathcal{L}$ with respect to $\mathbf{f}_{n+1}$ leads to the adjoint discrete equation in the form

$$\mathbf{p}^{\mathrm{T}}_n\boldsymbol{C}_{n+1} - \mathbf{p}^{\mathrm{T}}_{n+1}C^1_{n+2}\boldsymbol{B}_{n+1} - \mathbf{p}^{\mathrm{T}}_{n+2}C^2_{n+3}\boldsymbol{B}_{n+1} = 0, \tag{23}$$

where the solution at step n is obtained by marching upstream in space from the outlet to the inlet and needs two steps downstream to be computed.

V. Results

Results for both flat plate and sphere are discussed. For the flat plate case, all the results presented in Ref. 18 obtained there with a spectral collocation method (SCM) were repeated and the code verified against them (this verification is omitted here). Only original results regarding the use of the full energy norm (FEN) at the outlet are considered and compared to the partial energy norm (PEN). On the other hand, the code for optimal perturbations on the sphere was verified against Ref. 17 (SCM) and results are here presented for both partial and full energy norm at the outlet. The inlet norm is kept in the form (9), which encompasses v and w only.

The base flow for the flat plate is the same as in Ref. 18 and is obtained from a conventional similarity solution; for the case of the sphere, baseflow details can be found in Ref. 17.

A. Flat plate

Here we consider a perfect gas with a specific heat ratio $\gamma = 1.4$, Prandtl number $Pr = 0.7$ and viscosity depending on T only, in accordance with the Sutherland law. The stagnation temperature T_0 is fixed and equal to 333 K. Emphasis is on the use of the full energy norm at the outlet, which includes not only u and T (as done in Ref. 18) but also also v and w, as described in the section devoted to the optimization (§A).

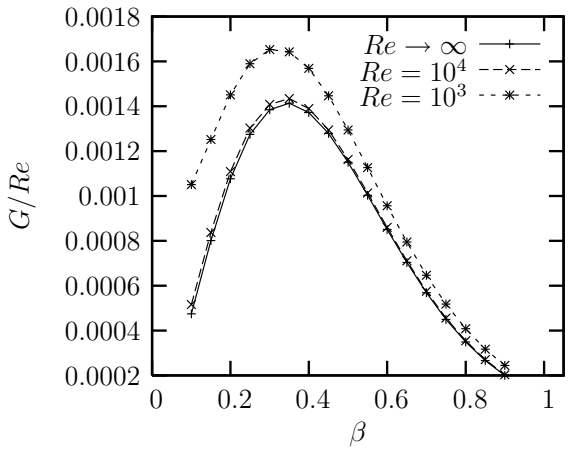

Figure 1. Objective function G/Re: effect of Re and β for $M = 3$, $T_w/T_{\rm ad} = 1$, $x_{\rm in} = 0$ $x_{\rm out} = 1.0$

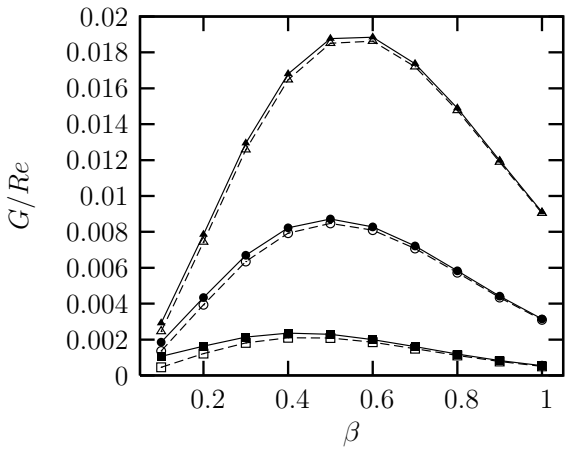

Figure 2. Objective function G/Re: effect of β, $T_w/T_{\rm ad}$ and norm choice Partial Energy Norm (PEN - only u^2 and T^2) Full Energy Norm (FEN) for $M = 0.5$, $Re = 10^3$, $x_{\rm in} = 0$ $x_{\rm out} = 1.0$. ×, PEN; □, $T_w/T_{\rm ad} = 1.00$; ○, $T_w/T_{\rm ad} = 0.50$; △, $T_w/T_{\rm ad} = 0.25$.

Figure 1 shows the effect of the Reynolds number Re on the gain G/Re, where $G = E_{\rm out}/E_{\rm in}$. The plot refers to the case Mach number $M = 3$, adiabatic wall, initial station for the computation $x_{\rm in} = 0$, and outlet station $x_{\rm out} = 1.0$. It is clear that the Reynolds number has quite a strong influence only for $Re < 10^4$, while for values greater than this limit, results do not differ significantly from the Reynolds-independent case.

The effect of the norm for different temperature factors $T_w/T_{\rm ad}$, where T_w is the wall temperature and $T_{\rm ad}$ the recovery temperature, at $M = 0.5$ is reported in figure 2 ($x_{\rm in} = 0$, $x_{\rm out} = 1.0$). The Reynolds number for the case of full energy norm is $Re = 10^3$. It can be concluded that at low Mach number $M = 0.5$, though large enough to allow compressible effects, the choice of the norm does not produce a remarkable difference.

The conclusion drawn from figure 2 does not extend to larger values of Mach number. In figure 3, a moderate supersonic Mach number $M = 1.5$ is considered. The effect of increasing M is clearly to shift the maximum of the curves towards smaller values of β and to enhance the difference between results obtained with different norms. This is particularly true for $T_w/T_{\rm ad} = 1.00$.

In the supersonic case, $M = 3$, reported in figure 4, a difference up to 17% can be detected when comparing PEN with FEN. This difference is remarkably higher for low values of the wavenumber β. Incidentally, this was visible also in figure 2 of Ref. 12 for $M = 0$.

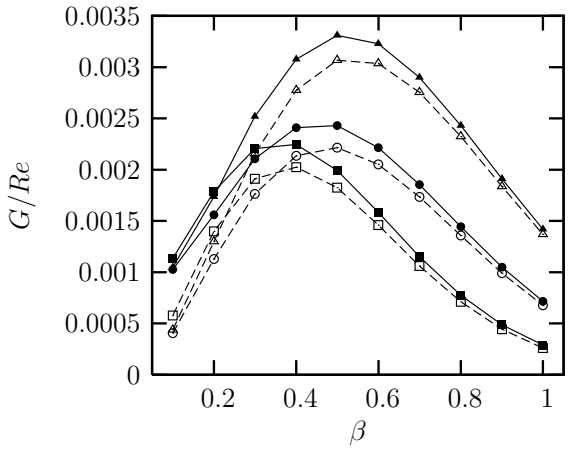

Figure 3. Objective function G/Re: effect of β, T_w/T_{ad} and norm choice Partial Energy Norm (PEN - only u^2 and T^2) Full Energy Norm (FEN) for $M = 1.5$, $Re = 10^3$, $x_{in} = 0$ $x_{out} = 1.0$. ×, PEN; □, $T_w/T_{ad} = 1.00$; ○, $T_w/T_{ad} = 0.50$; △, $T_w/T_{ad} = 0.25$.

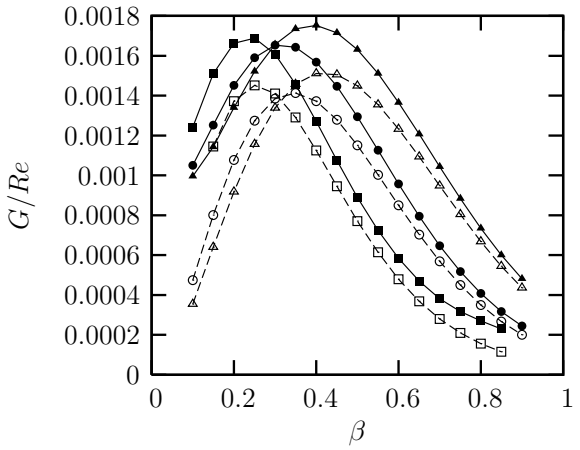

Figure 4. Objective function G/Re: effect of β, T_w/T_{ad} and norm choice Partial Energy Norm (PEN - only u^2 and T^2) Full Energy Norm (FEN) for $M = 3$, $Re = 10^3$, $x_{in} = 0$ $x_{out} = 1.0$. ×, PEN; □, $T_w/T_{ad} = 1.00$; ○, $T_w/T_{ad} = 0.50$; △, $T_w/T_{ad} = 0.25$.

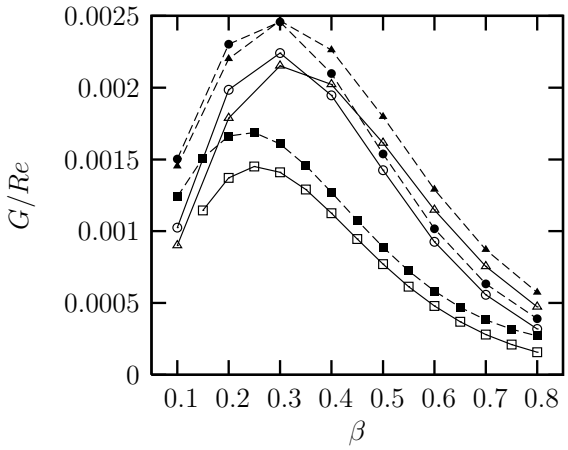

Figure 5. Objective function G/Re: effect of x_{in} and β and norm choice Partial Energy Norm (PEN - only u^2 and T^2) Full Energy Norm (FEN) for $M = 3$, $T_w/T_{ad} = 1$, $x_{out} = 1.0$. □, $x_{in} = 0.0$; ○, $x_{in} = 0.2$; △, $x_{in} = 0.4$; full symbols refer to FEN, empty ones to PEN.

A further comparison between the use of full or partial energy norm at the outlet is shown in figure 5. Curves differ not only because of the energy norm but also for the initial location x_{in}, which ranges from 0 to 0.4. As reported in Ref. 17, moving x_{in} downstream produces a much higher energy growth. From figure 5, however, it can be noticed that the significant difference observed between comparing the cases $x_{in} = 0.0$ and $x_{in} = 0.2$ is no more present when comparing results for $x_{in} = 0.2$ and $x_{in} = 0.4$. The use of the full energy norm (as opposed to the partial energy norm), provides an energy growth much larger than in all previous cases, where different Mach numbers and temperature factors where considered. For $x_{in} = 0.4$ and $\beta = 0.1$ this difference is on the order of 62%.

Velocity profiles for these conditions ($M = 3.0$, $Re = 10^3$, $x_{in} = 0.4$, $x_{out} = 1.0$ and $\beta = 0.1$) are reported in figures 6 and 7, where FEN is compared with PEN. Optimal perturbations at $x_{in} = 0.4$ (figure 6) reveal that the use of the full energy norm does not produce significant changes in v, while more discrepancies are seen in w. On the other hand, outlet profiles (figure 7) for the full energy norm case show a larger effect on v, rather than on w. Profiles of u and T at the outlet are not reported because there is not a significant effect on them (as expected).

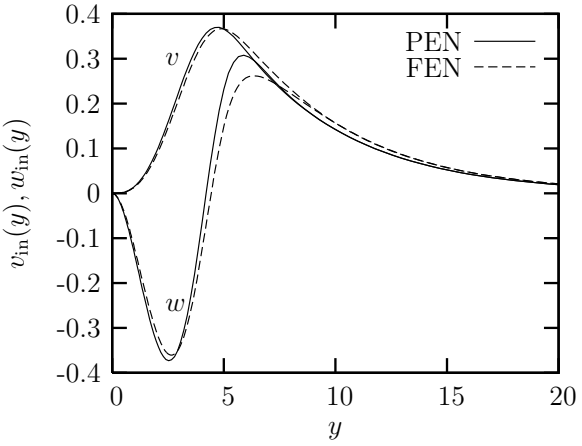

Figure 6. Optimal perturbations at $x_{\rm in} = 0.4$: effect of norm choice Partial Energy Norm (PEN - only u^2 and T^2) Full Energy Norm (FEN) for $M = 3.0$, $Re = 10^3$, $x_{\rm in} = 0.4$ $x_{\rm out} = 1.0$ and $\beta = 0.1$.

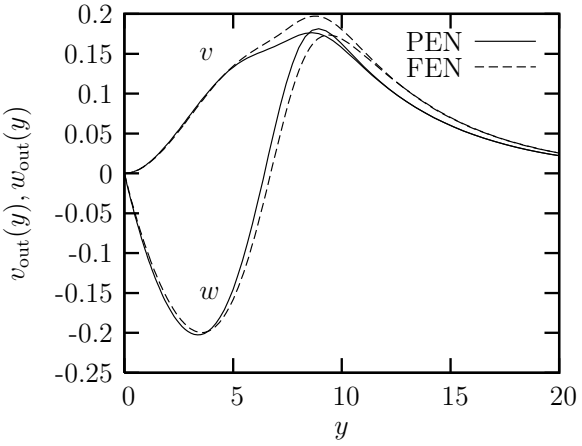

Figure 7. Outlet profiles at $x_{\rm out} = 1.0$: effect of norm choice Partial Energy Norm (PEN - only u^2 and T^2) Full Energy Norm (FEN) for $M = 3.0$, $Re = 10^3$, $x_{\rm in} = 0.4$ $x_{\rm out} = 1.0$ and $\beta = 0.1$.

For the flat-plate case it can be concluded that an energy norm including v and w at the outlet provides a significant difference with respect to the case where only u and T are considered and that this effect increases with the Mach number and $x_{\rm in}$.

B. Sphere

Figure 8 provides an example of comparisons between present results and previously published ones[17] (θ denotes the meridional angle, which is associated with the streamwise direction). It goes without saying that the agreement is extremely good, but the purpose of the figure is not to show the agreement, rather to provide better insights regarding the dependence of G on the the choice of $\theta_{\rm in}$ and $\theta_{\rm out}$ (respectively inlet and outlet locations). It can be noticed that when the range of θ is small the gain is the largest. The difference $\theta_{\rm out} - \theta_{\rm in}$, however, is not the only factor that causes a larger energy growth. In fact, curves with the same $\theta_{\rm out} - \theta_{\rm in}$ (5 deg) but with different $\theta_{\rm in}$ clearly show that the strongest transient growth is achieved close to the stagnation point.

However, the main outcome from figure 8 seems to be that the divergence of the flow caused by the spherical geometry is responsible for large transient energy growth in the proximity of the stagnation point. Moreover, this effect is much stronger when the difference $\theta_{\rm out} - \theta_{\rm in}$ is small. Due to the short downstream development of the flow, one issue is that maybe the optimal perturbation in the form of counter rotating vortices still dominates the flow field and therefore the choice of the partial energy norm at the outlet could be misleading. On the contrary, the use of the full energy norm (which encompasses not only u and T but also v and w) at the outlet would clarify this issue.

Figure 9 shows the effect of norm choice and ϵ. Quite a number of curves are reported because comparisons of FEN have meaning depending on the value of ϵ, but results with the PEN change with ϵ as well. The constant parameters are $\theta_{\rm in} = 2.0$ deg, $\theta_{\rm out} = 5.0$ deg $\theta_{\rm ref} = 30.0$ deg and $T_w/T_{\rm ad} = 0.5$. For $\epsilon = 10^{-3}$ there is basically no difference between using PEN and FEN. However, it is precisely in this range of ϵ that it is meaningful to investigate the behavior of the solution, since it corresponds to the estimate values for wind tunnel conditions and flight tests, as reported in figures 6 and 7 of Ref. 17. For higher values of ϵ the difference between the use of the two norms seems to be more evident.

The conclusion from figure 9 is, however, that the maximum appreciable difference is confined to within about 1% of the parameters of interest.

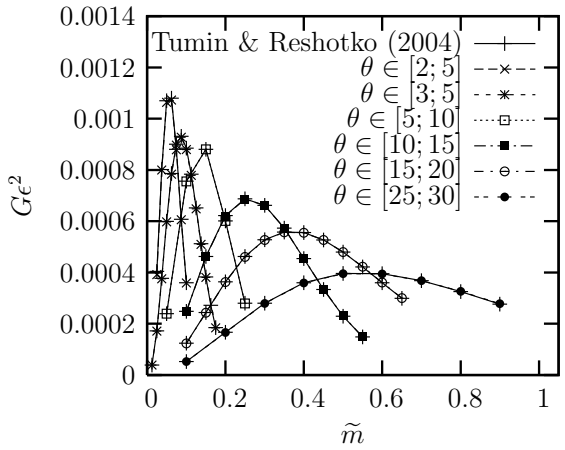

Figure 8. Objective function $G\epsilon^2$: effect of interval location and $\widetilde{m}$ for $\theta_{\text{ref}} = 30.0$ deg, $T_w/T_{\text{ad}} = 0.5$, $\epsilon = 10^{-3}$. PEN.

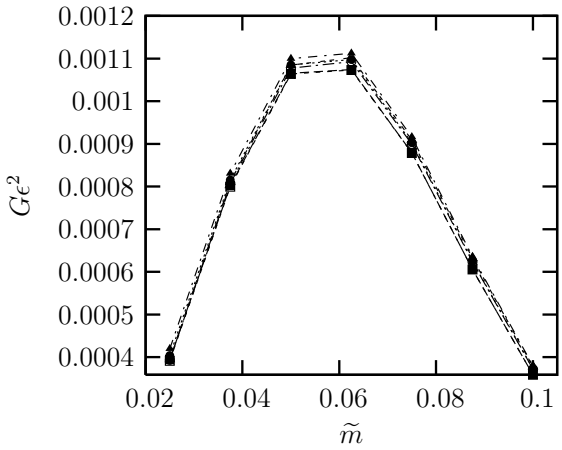

Figure 9. Objective function $G\epsilon^2$: effect of ϵ, energy norm (FEN = Full Energy Norm; PEN = Partial Energy Norm) and $\widetilde{m}$ for $\theta_{\text{in}} = 2.0$ deg, $\theta_{\text{out}} = 5.0$ deg, $\theta_{\text{ref}} = 30.0$ deg, $T_w/T_{\text{ad}} = 0.5$. □, $\epsilon = 1{\cdot}10^{-3}$; ○, $\epsilon = 2{\cdot}10^{-3}$; △, $\epsilon = 3 \cdot 10^{-3}$; full symbols refer to FEN, empty ones to PEN.

VI. Conclusions

Optimal perturbations in the compressible regime have been considered for both flat plate and sphere. An adjoint-based optimization technique is employed and the discrete costate problem is obtained from the discretized direct problem by applying the Lagrangian multipliers technique in the discrete framework. This simplifies the code, reduces the number of possible errors, and allows the automatic generation of coupling conditions at the inlet and outlet. The code has been verified against available results.[18,17]

The main contributions of the present work are the analysis including the full energy norm at the outlet and the fully discrete approach (including the coupling conditions), which considerably facilitates its implementation. In previous works regarding compressible optimal disturbances the quantity that was maximized was always an incomplete Mack's norm, including only u and T in the fashion proposed by Luchini[13] in the incompressible case. This norm, however, does not consider the effect of v and w at the outlet, because they scale with the Reynolds number and therefore are neglected as they are much smaller than u and T.

Results for the flat plate show that when the Reynolds number is on the order of 10^3, a significant difference in the energy growth (up to 62%) is found between the two choices of the outlet energy norm (full or partial). This is particularly true for supersonic Mach numbers and downstream locations of the initial point for the calculation ($x_{\text{in}} = 0.4$). On the other hand, when compressible effects are considerable but the basic flow is subsonic, the difference between the full and partial energy norms is not a critical factor. If the Reynolds number is greater than 10^4, v_{out} and w_{out} do not play a significant role even in supersonic flows.

Results for the sphere show that the largest gain occurs close to the stagnation point and for a small range of the meridional angle, raising the issue of the use of a full energy norm at the outlet in order to account for the possibly still undeveloped streaky structure of the perturbation field. Results reveal that, in the range of interesting values of Re_{ref} (related to the small parameter $\epsilon = Re_{\text{ref}}^{-1/2}$) that are typical of wind tunnel tests or flight conditions ($\epsilon = \mathcal{O}(10^{-3})$), no significant role is played by v and w at the outlet.

Acknowledgment

This work was supported by the U.S. Air Force Office of Scientific Research.

References

[1]Reshotko, E., "Transient growth: a factor in bypass transition," *Phys. Fluids*, Vol. 13, 2001, pp. 1067–1075.

[2]Ellingsen, T. and Palm, E., "Stability of linear flow," *Phys. Fluids*, Vol. 18, 1975, pp. 487–488.

[3]Landahl, M. T., "A note on an algebraic instability of inviscid parallel shear flow," *J. Fluid Mech.*, Vol. 98, 1980, pp. 243–251.

[4]Hultgren, L. S. and Gustavsson, L. H., "Algebraic growth of disturbances in a laminar boundary layer," *Phys. Fluids*, Vol. 24, No. 6, 1981, pp. 1000–1004.

[5]Farrell, B., "Optimal excitation of perturbations in viscous shear flow," *Phys. Fluids*, Vol. 31, No. 8, 1988, pp. 2093–2102.

[6]Boberg, L. and Brosa, U., "Onset of turbulence in a pipe," *Z. Natursforschung*, Vol. 43a, 1988, pp. 697–726.

[7]Butler, K. M. and Farrell, B., "Three–dimensional optimal perturbations in viscous shear flow," *Phys. Fluids A*, Vol. 4, 1992, pp. 1637–1650.

[8]Gustavsson, L. H., "Energy growth of three-dimensional disturbances in plane Poisuille flow," *J. Fluid Mech.*, Vol. 224, 1991, pp. 241–260.

[9]Reddy, S. C. and Henningson, D. S., "Energy growth in viscous channel flows," *J. Fluid Mech.*, Vol. 252, 1993, pp. 209–238.

[10]Trefethen, L. N., Trefethen, A. E., Reddy, S. C., and Driscoll, T. A., "Hydrodynamic Stability without Eigenvalues," *Science*, Vol. 261, 1993, pp. 578–584.

[11]Tumin, A. and Reshotko, E., "Spatial Theory of optimal disturbances in boundary layers," *Phys. Fluids*, Vol. 13, No. 7, 2001, pp. 2097–2104.

[12]Andersson, P., Berggren, M., and Henningson, D. S., "Optimal disturbances and bypass transition in boundary layers," *Phys. Fluids*, Vol. 11, 1999, pp. 134–150.

[13]Luchini, P., "Reynolds–number–independent instability of the boundary layer over a flat surface: optimal perturbations," *J. Fluid Mech.*, Vol. 404, 2000, pp. 289–309.

[14]Zuccher, S., Luchini, P., and Bottaro, A., "Algebraic growth in a Blasius boundary layer: optimal and robust control by mean suction in the nonlinear regime," *J. Fluid Mech.*, Vol. 513, 2004, pp. 135–160.

[15]Hanifi, A., Schmidt, P. J., and Henningson, D., "Transient growth in compressible boundary layer flow," *Phys. Fluids*, Vol. 8, No. 3, 1996, pp. 51–65.

[16]Reshotko, E. and Tumin, A., "The blunt body paradox – A case for transient growth," *Laminar–Turbulent Transition*, Springer–Verlag, Berlin, 2000, pp. 403–408, Paper presented at the 5th IUTAM Symposium on Laminar-Turbulent Transition, Sedona, USA, 1999.

[17]Tumin, A. and Reshotko, E., "Optimal disturbances in the boundary layer over a sphere," AIAA Paper AIAA–2004–2241, 2004.

[18]Tumin, A. and Reshotko, E., "Optimal disturbances in compressible boundary layers," *AIAA J.*, Vol. 41, No. 12, 2003, pp. 2357–2363.

[19]Reshotko, E. and Tumin, A., "The role of transient growth in roughness-induced transition," *AIAA J.*, Vol. 42, No. 4, 2004, pp. 766–770.

[20]Cathalifaud, P. and Luchini, P., "Algebraic growth in boundary layers: optimal control by blowing and suction at the wall," *Eur. J. Mech. B – Fluids*, Vol. 19, 2000, pp. 469–490.

[21]Zuccher, S., Bottaro, A., and Luchini, P., "Algebraic growth in a Blasius boundary layer: nonlinear optimal disturbances." *Eur. J. Mech. B/Fluids*, 2004, (Submitted).

[22]Mack, L. M., "Boundary Layer Stability Theory," JPL Report 900-277, Jet Propulsion Lab., California Institute of Technology, Pasadena, CA, USA, 1969.

[23]Naylor, A. W. and Sell, G. R., *Linear Operator Theory in Engineering and Science (Applied Mathematical Sciences, Vol 40)*, Springer, 2000.

[24]Kreyszig, E., *Introductory functional analysis with applications*, John Wiley & Sons, 1989.

[25]Luchini, P. and Bottaro, A., "Görtler vortices: a backward–in–time approach to the receptivity problem," *J. Fluid Mech.*, Vol. 363, 1998, pp. 1–23.

[26]Luchini, P. and Bottaro, A., "Linear stability and receptivity analyses of the Stokes layer produced by an impulsively started plate," *Phys. Fluids*, Vol. 13, 2001, pp. 1668–1678.

[27]Gunzburger, M., "Adjoint equation-based methods for control problems in incompressible, viscous flows," *Flow, Turb. & Comb.*, Vol. 65, 2000, pp. 249–272.